

CEBAF Program Advisory Committee Six (PAC6) Proposal Cover Sheet

This proposal must be received by close of business on April 5, 1993 at:

CEBAF
User Liaison Office
12000 Jefferson Avenue
Newport News, VA 23606

Proposal Title

DEUTERON PHOTODISINTEGRATION BY LINEAR
POLARIZED PHOTONS

Contact Person

Name: V. B. GANENKO
Institution: KHARKOV INSTITUTE OF PHYSICS + TECH
Address: AKADEMICHESKAJA ST., 1, KHARKOV, 310108, UKRAINE
Address:
City, State ZIP/Country: KHARKOV, UKRAINE
Phone: (057) 235-1993 FAX: (057) 235-1738
E-Mail → BITnet: KFTI@KFTI.KHARKOV.UA Internet:

If this proposal is based on a previously submitted proposal or
letter-of-intent, give the number, title and date:

PR 91-012
PR 93-004

CEBAF Use Only

Receipt Date: 4/14/92 Log Number Assigned: 94-022

By: to [signature]

Deuteron photodisintegration by linear polarized photons

Abstract

We propose to measure the asymmetry of the $\gamma d \rightarrow pn$ cross section in the photon energy range $E_\gamma = 0.6 \rightarrow 2.4$ GeV. The measurements will be carried out with a linearly polarized photon beam, which is obtained in the course by coherent bremsstrahlung of relativistic electrons in a diamond crystal. These measurements will allow one :

- to check the predictions of the available theoretical models of the $\gamma d \rightarrow pn$ process in the energy range of $1 \rightarrow 2$ GeV;

- to clarify whether quark mechanisms or hadron mechanisms determine $\gamma d \rightarrow pn$ in this energy range;

- to determine the possible addition of nonnucleon (N^*) configurations in the deuteron wave function and their characteristics;

- to check, using new experimental data, the phenomenon of asymptotic scaling in $\gamma d \rightarrow pn$ predicted in [3 - 6] and observed in SLAC experiments [1,2].

The experiment will be a part of the program for studying $\gamma d \rightarrow pn$ proposed for CEBAF [7,8].

Introduction

For more than fifty years deuteron photodisintegration

$$\gamma d \rightarrow pn \tag{1}$$

has attracted great deal of attention, since it is the simplest nuclear process whose studying allows one to check fundamental ideas of nuclear and elementary particle physics.

At present time the photon energy range $E_\gamma \geq 1$ GeV is the most interesting for studying. In this range the reaction mechanisms are complicated and, apparently, substantially evolve with increasing energy. Recent measurements performed at SLAC [1,2] show that at energies $E_\gamma \geq 1.4$ GeV mechanisms of the reaction caused by quark configurations are possible. At the same time according to theoretical computations [9,11] the data of refs. [1,2] can be satisfactorily described within the framework of the meson - nucleon theory up to the energy $E_\gamma \approx 2$ GeV. At higher energy ($E_\gamma \approx 2.4$ GeV) a change in the reaction mechanism is possible, and the description of the process using QCD may be more adequate.

One should expect that qualitatively new information on the process (1) in the range of energy higher than 1 GeV can be obtained by studying polarized observables which are often more sensitive to the details of the mechanism than cross sections. In particular, it is important to study the asymmetry of the reaction (1) cross section:

$$\Sigma = \frac{d\sigma_{\parallel} - d\sigma_{\perp}}{d\sigma_{\parallel} + d\sigma_{\perp}} \tag{2}$$

where $d\sigma_{\parallel(\perp)} = d\sigma_{\parallel(\perp)}/d\Theta$ is the cross section in the case when the photon polarization vector is parallel (perpendicular) to the reaction plane. First, according to [9], the model of refs. [3-6] and the meson theory give qualitatively different predictions. Second, the

asymmetry for photon energies from 1 → 2 GeV is very sensitive to the presence of nucleon configurations in the deuteron wave functions and excitation of nucleon resonances.

This experiment is relatively simple. It does not require :

- high electron currents;
- complicated detector systems for reaction product detection;
- performing absolute measurements.

Hence, the experiment can be run at the first stage of the development of experimental methods and the use of the CEBAF accelerator.

Physics Motivation

Constituent counting rules

At present time quantum chromodynamics describes well enough a number of hard processes. For instance, constituent counting rules [3-6] predict, at high energies, a definite behavior of hardron formfactors and the cross sections of exclusive reactions. In particular, the dependence of the differential cross sections on the total energy squared s at a fixed value of the angle θ_p^{cm} in the center-of-mass system is predicted to have the form:

$$\frac{d\sigma}{dt} \approx s^{n-2} \quad (3)$$

where n is the total number of quarks, photons, and other fundamental particles in the initial plus final states in the reaction. This prediction of the quark models has been confirmed by experiments on NN scattering and pion photoproduction, $\gamma N \rightarrow \pi N$. The scaling dependence of $pp \rightarrow pp$ and $\gamma N \rightarrow \pi N$ cross sections has been observed at high energies of incident particles ($s/m^2 \geq 15$ and 7 for the first and the second reactions, respectively, where m is the nucleon mass), and in the case of $pp \rightarrow pp$ scattering the phenomenon has been observed in a wide range of angles (Fig.1). The dependence of π , p and n form factors on Q^2 also agrees with the theory quite well. Concerning the reaction (1) , a hint of scaling behavior of the cross section was obtained in the first SLAC experiment [1] at comparatively low energies $E_\gamma \approx 1.4\text{GeV}$ ($s/M_d^2 \approx 2$, where M_d is deuteron mass). The data of ref. [1] and preliminary results of the second SLAC experiment [2] show that for $\theta_p^{cm} = 53^\circ$ and 90° the cross section energy dependence is described by Eq. (3) ,($n = 12.1 \pm 0.8$ for $\theta_p^{cm} = 90^\circ$ and $n = 11.0 \pm 0.5$ for $\theta_p^{cm} = 53^\circ$) starting with $E_\gamma \approx 1 \rightarrow 1.2$ GeV, (Fig.2).

However, the data for $\theta_p^{cm} = 37^\circ$ essentially differ from the predictions of the constituent counting rules. The dependence observed is also of the form (3) , but $n = 8.7 \pm 0.3$ (Fig.2c). This result points either to the variation, with the proton production angle, of the number of interacting elementary fields in the reaction (1) ,or, more probably, points out that at present time it is not clear what factors (quarks or nucleons) cause the behavior of the process (1) cross section in the energy range of 1 → 2 GeV. Thus, the prediction of asymptotic scaling in the reaction (1) requires experimental confirmation.

Meson theory

There are yet a number of theoretical calculations [9,10,11], in which the attempts of the data SLAC [1,2] in the energy range $E_\gamma \geq 1$ GeV have been done within the framework of the conventional meson theory.

The analysis and comparison of the SLAC experimental data with the results of calculation of ref. [10] carried out in ref.[2] have shown that the results of [10] do not agree

with the experimental data for practically all angles at $E_\gamma \geq 1$ GeV, (Fig.3). The most considerable disagreement is for $\theta_p^{cm} \leq 53^\circ$.

In ref. [11] calculation of differential cross section and polarization observables Σ, P_y, T of the reaction $\gamma d \rightarrow pn$ have been carried out in the energy range up to 1.6 GeV. In these calculations Hulthen wave function was used the exchange of π, ρ, η mesons, final state interaction and also the excitation of virtual Δ and other nucleon resonances with $J \leq 5/2$ and mass up to 2 GeV were taken into account. The results shows good agreements with the SLAC experimental data for $\theta_p^* = 90^\circ$ and $\theta_p^* = 143^\circ$ and the energy range up to 1.6 GeV and it is important that nucleon resonances play important role for getting agreement of experiment and theory, Fig.4c.

Some another model were used in [9], where a detailed study of the reaction (1) at $E_\gamma > 1$ GeV was carried out in a Lorentz-covariant approach. The deuteron wave function used for the computation contained nucleon $|NN\rangle$ and Roper configurations. ($N(\frac{1}{2}^+, 940)$ stands for the nucleon and $N^*(\frac{1}{2}^+, 1440)$ stands for the Roper resonance). The model of ref. [12] was used as the dynamical model of dNN and dNN* vertices. It was assumed that for dNN and dNN* the rates of the form factor decrease are equal and described by the following expression:

$$G(-k^2)_{N(N^*)} = C_{N(N^*)} [\beta_{N(N^*)}^2 / 2 + \alpha_0^2 - k^2]^{-\epsilon} \quad (4)$$

The rate of formfactor decrease is described by one parameter $\epsilon = 3; \epsilon = 4$ corresponds to the asymptotic condition. The values of other parameters, which are the same for the NN and NN* configurations, are: $\alpha_0^2 = 0.002m^2$, where m is the nucleon mass, and $\beta^2 = 0.02m^2$. The ratio of dNN to the dNN* vertex form factor (in the asymptotic region of the theory) is determined by a single parameter $\alpha = C_{N^*}/C_N$. The value of C_N was fixed by matching the theoretically calculated cross section to the experimental data [1] at $E_\gamma = 1$ GeV and $\theta_p^{cm} = 90^\circ$.

The results of theoretical calculations [9] of the differential cross section are shown in Fig.4a. Continuous curves 1 and 2 correspond to the calculations without taking into account the NN* configurations ($\alpha = 0$). Curve 2, corresponding to the asymptotic case ($\epsilon = 4$), is in good agreement with the result of ref. [13] (crosses), which assume scaling behavior for the process amplitudes. The dashed curve was obtained by taking into account the NN* configurations with $\alpha = 15$ and $\epsilon = 3$. One can see that for $\theta_p^{cm} = 90^\circ$, the SLAC experimental data [1,2] are in rather good agreement with the predictions of meson theory [9] up to the photon energies of $E_\gamma \approx 2.2 \rightarrow 2.4$ GeV, when the NN* configurations are taken into account in the dNN and dNN* vertex models [12]. At higher energies, considerable disagreement of the theoretical calculations at $\epsilon = 3$ with the experiment is seen. Better agreement is obtained when the asymptotic behavior ($\epsilon = 4$) of the dNN vertex formfactor is assumed. According to [9] in the region $E_\gamma \geq 2.4$ GeV the behavior of the amplitudes seems to change, and the scaling predicted in [3-6] can exist at energies above 2.4 GeV.

One of the important conclusions of [9] is that in the framework of meson-nucleon theory one can get, for large s , a factorized form of the reaction (1):

$$\frac{d\sigma}{d\Omega} \approx \text{const} * f(\theta, s) / s(s-1)^{2\epsilon-1} \quad (5)$$

which, for $\theta_p^{cm} = 90^\circ$, $f(90^\circ, s) = 1$, and at $\epsilon = 3$ in the energy range $E_\gamma = 1 \rightarrow 3$ GeV

($s = 8 \rightarrow 16$ GeV), can imitate the energy dependence of the cross section in the form:

$$\frac{d\sigma}{dt} \approx s^{-11-12} \quad (6)$$

which coincides with that predicted by the constituent counting model [3 - 6]. Hence, within 1-3 GeV region the cross section energy dependence (6) itself can not be considered as the serious argument for the QCD mechanisms of real photon absorption in this energy range. To solve the problem data on other observables are required.

Another important conclusion of [9] is that $f(\theta, s)$, (where only the NN configuration is taken into account) is almost independent of s only in the angle interval:

$$50^\circ \leq \theta_p^{cm} \leq 130^\circ \quad (7)$$

Thus, the energy dependence (6) can take place only within this angle interval. Beyond the interval (7) the rate of cross section falloff with varying s decreases, and $s^{11} \cdot d\sigma/dt$ becomes an increasing function with the rate of increase being higher in the region of forward scattering angles than in the region of backward scattering angles. The SLAC experimental data [1,2] qualitatively confirm this conclusion (Fig.4b).

Apparently, the model [9] provides a correct general picture of the process, at least for energies up to $2.4 \rightarrow 3.0$ GeV. If it is true, the photon interacts with nucleons and not with quark configurations, and the scaling is not observed for this energy region.

Fig.5a presents the results of calculations of the cross section (2) asymmetry for $\theta_p^{cm} = 90^\circ$. The dotted curve corresponds to the case when only the NN configurations are taken into account in the deuteron wave function. Curves 1,2,3 and 4 for $\alpha = 10, 15, 20$ and 30 , respectively, correspond to the case when the NN* are taken into account. One can see that in accordance with [9] the asymmetry is very sensitive to the presence in the deuteron ground state of the addition of resonance configurations. The inclusion of the latter results in a factor of several decrease in the asymmetry magnitude. Theory predicts the most abrupt change in the asymmetry behavior for $\theta_p^{cm} \leq 60^\circ$, where the asymmetry magnitude decreases from 0.7 to ≈ 0 . (Fig.5b). This effect is a general consequence of the presence in the deuteron of the non-nucleon configurations.

In contrast to the cross section the asymmetry is weakly dependent on the rate of the formfactor falloff in the dNN vertex.

The calculations of ref.[11] predict for Σ qualitatively different energy dependence in the energy range $E_\gamma \geq 0.6$ GeV then [9]. While [9] predict smooth energy dependence, decreasing with energy increase the calculations [11] predict presence of the some structures at energies $E_\gamma \approx 0.8$ and 1.2 GeV and strong dependence of value of the Σ asymmetry from nucleon resonances contribution, Fig.5c. The experimental data [14], obtained at $E_\gamma \leq 1$ GeV are in good agreement with theoretical calculations [9].

It is very important that the predictions of the model [9] and of the constituent counting model [3-6] for the asymmetry at $\theta_p^{cm} = 90^\circ$ and in the energy range $1 \rightarrow 3$ GeV are essentially different. The expected value of the Σ asymmetry in the asymptotic scaling mode is:

$$\Sigma \approx -1 \quad (8)$$

independent of the deuteron structure, while the model [9] predicts, under the same conditions, the asymmetry value to be close to zero. Thus, the measurement of the asymmetry may become a strong criterion for the presence or absence of the asymptotic

scaling. It will allow one to answer the question of whether or not quark states of freedom manifest themselves in deuteron photodisintegration in the given energy region.

According to [9] the theoretical parameter α can be expressed through such physical parameters as the mean square radii r_N and r_{N^*} of the NN and NN^* configurations and the admixture of the NN^* component in the deuteron:

$$\alpha \approx \left(\frac{\xi}{1-\xi} \right)^{1/2} \left(\frac{r_N}{r_{N^*}} \right)^{5/2} \left(\frac{m}{M_{N^*}} \right)^{1/2} \left(\frac{m + M_{N^*}}{2m} \right) \quad (9)$$

where ξ is the admixture of the NN^* configuration in the deuteron wave function, and m and M^* are the nuclear mass and the nucleon resonance mass, respectively. The comparison of the calculations with experimental data [14] restricts α values to be from 10 to 15. In [9], with taking $r_N \approx 2$ fm and assuming that NN^* admixture is about 2 %, it was found that the NN^* configuration radius is within the following interval:

$$0.33 \leq r_{N^*} \leq 0.38 \text{ fm} \quad (10)$$

This is in good agreement with the nuclear core radius in NN potentials.

The estimates of the role of the off-shell effects carried out in [9] shown that these effects are not able to shadow the non-nucleon component effects in the deuteron wave function.

Thus, the asymmetry measurement in a region of $1 \rightarrow 2$ GeV will allow one to check the theoretical predictions of meson theories [9,11] and, if the [9] gives the correct description of the process (1), to study the non-nucleon configurations in the deuteron wave function.

General description of proposed experiment

We propose to measure the energy dependence of the cross section asymmetry of the $\gamma d \rightarrow pn$ in the photon energy range $E_\gamma = 0.6 \rightarrow 2.4$ GeV at $\theta_p^{cm} = 30^\circ, 90^\circ$ and 150° , and to measure angular distributions for $E_\gamma = 1.0, 1.4$ and 2.0 GeV.

The experiment will be carried out with a linearly polarized photon beam obtained by the interaction of electrons with a diamond single crystal. The separation of the reaction under investigation from competing processes will be performed with the help of pn coincidence measurements.

Because of a considerable decrease in the reaction cross section with increasing energy, running the experiment requires high luminosity and equipment which is capable to operating under the conditions of high counting rate. Hence, in the nearest time the measurements at energies above 1.5 GeV can be performed only at CEBAF in Hall A or C. Since in these Halls there is no equipment for the generation of pure photon beams we propose to develop a compact magnetic system for spatial separation of the γ and e^- beam and to run the experiment with the pure photon beam.

One of the conditions substantially simplifying the problem is that the proposed experiment does not imply using electron currents above $30 \mu\text{A}$.

Experimental set up

The experimental set up is shown in Fig.6. The electron beam strikes a diamond single crystal target, which it is suitably fixed in a goniometer, for producing polarized photons.

The goniometer setup is placed at a distance of $3 \rightarrow 3.5$ m from the deuteron target before the second raster magnet. Immediately behind the goniometer a magnetic system

with two dipole magnets is located. The system shifts the electrons, which have passed through the crystal, in the transverse direction. It is designed in such a way that the electrons with maximum energy are shifted by 10 → 12 mm and guided, in parallel to the incoming beam axis, beside the deuteron target into the beam dump.

After passing through the crystal the electron beam has an energy spectrum from 0 to E_0 ; it is not monochromatic. However, in contrast to the photon component the spectrum of energy of the scattered electrons has a maximum near the maximum energy E_0 (Fig. 7). The calculation performed for a crystal of thickness 0.5 mm, a beam current of $30\mu A$ and an initial energy of $E_0 = 4$ GeV shows that $\approx 97\%$ of the energy of the beam scattered electrons is contained in the spectrum range from 2 to 3.975 GeV and 98.3% of the energy is in the interval from 1.5 to 3.975 GeV (the total power of the scattered beam is ≈ 2000 W). Thus, when the energy acceptance of the system is $(0.5 \rightarrow 1) * E_0$, the scattered power not accepted by the system is $\approx 3\%$ (i.e. ≈ 60 W), and it is 1.7% (≈ 30 W) at an acceptance of $(0.375 \rightarrow 1) * E_0$.

Fig.8 demonstrates the geometry and the dimensions of the electron and photon beam for one of the types of the symmetrical magnetic system designed with the "Transport" program. The system consists of two identical dipole magnets with cut angles of the incoming and outgoing bound of $\approx 33^\circ$ and a gap of 10 mm. The magnetic field is 10 kG, the length of the magnetic pathway for the beam particles with an energy of 4 GeV is 25.8 cm and the distance between the magnets is 25.8 cm. The energy acceptance of the system is from 1.5 to 4 GeV. The system shifts the main particle by 10 mm and has the focal point at a distance of ≈ 15 m from the outgoing cut of the second magnet. At calculations, the electron beam entering the magnetic system (after the crystal) was assumed to have a dimension of ± 1 mm and an angular divergence of 0.16 mrad caused mainly by multiple scattering in 0.5 mm thick diamond. The divergence of the electron beam striking the crystal was assumed to be 0.1 mrad.

Thus, upon passing through the magnetic system the photon and electron beam are separated and move in the same vacuum pipe at a small distance from each other. Only the photon beam strikes the deuteron target. At the vicinity of the target the vertical dimensions of the beams do not exceed 3 → 4 mm, the maximum horizontal dimension at the exit of the magnetic system does not exceed 21-22 mm.

The cost of the by-pass system and shielding are not expensive and more less than cost of the saved beam time in experiments with mixed $\gamma + e^-$ beam.

2. Experimental technique and procedure

In the present variant of the experiment in Hall A the deuteron target is irradiated only by photons. Hence, the experimental procedure becomes simple.

i) Single crystal target. Spectra and polarization.

As the photon target we use the diamond crystal, which is most often used for getting polarized photon beams due to its high Debye temperature. The optimum thickness of the crystal is 0.5-1 mm. Fig.9 shows the photon spectra and polarization expected in the case where the single crystal target is oriented relative to the electron beam in such away that the main contribution to the coherent bremsstrahlung cross section is made by a single reciprocal lattice point $(2, \bar{2}, 0)$. Initial electron energy is $E_0 = 4$ GeV. $(2, \bar{2}, 0)$ orientation is most often used in experiments, since it allows one to obtain higher polarization than one obtains in the other possible orientations. The expected polarization varies from

≈ 0.65 at $E_\gamma=1$ GeV to ≈ 0.22 at $E_\gamma=2.4$ GeV. To prevent a considerable decrease in the coherent effect, which reduces the radiation polarization, the angular divergence of the electron beam θ_r should be several times less than the multiple scattering angle θ_{sc} .

$$\theta_r \leq \theta_{sc}$$

For the 1 mm thick crystal the limit on angular divergence is about 0.1 mrad.

ii) Single crystal orientation

Crystal orientation is a procedure of the preparing goniometer facility to measurements which consist in aligning one of the main crystal axis, for example $\vec{B}_1 = \langle 110 \rangle$, with the beam axis \vec{P}_0 , and the two other axes $\vec{B}_2 = \langle 1\bar{1}0 \rangle$ and $\vec{B}_3 = \langle 001 \rangle$ with the horizontal and vertical rotation axis of the goniometer. When performing the procedure one usually makes special measurements of the orientation dependence of the photon beam intensity with an ionization chamber or a quantometer. In Hall A there is no magnet to clean the photon beam from the charged component, but supposed magnetic system which separate γ and e^- beams in Hall A allows to carry out such measurements with conventional method with small ionization chamber.

We suppose to use in the experiment new automatized goniometer system developed by our group in KhFTI. Essential peculiarity of this goniometer is the availability additional axis of the rotation around the beam axis \vec{P}_0 . It allows one to change quickly the direction of photon polarization relative reaction plane without changing spectrum of the intensity of the coherent bremsstrahlung. We can use two conditions of operation-discrete and uninterrupted rate of the rotation of the polarization vector around beam axis. That goniometer system allows to eliminate systematic errors connected with possible fluctuation of the parameters of the beam and apparatus.

Besides using this system we can decrease radiation damage of the single crystal target without raster magnets and can increase its life time.

Precision of the angle reading of the goniometer for rotation around vertical and horizontal axes are $5 \cdot 10^{-5}$ rad, around the beam axis is 0.1° .

iii) Determining the polarization

We suppose to determine the degree of photon polarization in the region of the maximum of the coherent peak by measuring the orientation dependence of the reaction (1) yields $C_{\parallel(\perp)}(\theta_p, P_p; \theta_{cr}, \alpha)$ (for photons polarized parallel and perpendicular to the reaction plane) at fixed values of the kinematic parameters θ_p and P_p (the angle and the momentum of the outgoing proton) corresponding to the chosen value of photon energy. θ_{cr} and α are crystal orientation angles (θ_{cr} is the angle between the electron momentum \vec{P}_0 and \vec{B}_1 axis and α is the angle between planes (\vec{P}_0, \vec{B}_1) and (\vec{B}_1, \vec{B}_2)). These angles unambiguously determine the location of the interference peak E_γ^p in the spectrum of coherent bremsstrahlung. In the case when the main contribution into the coherent bremsstrahlung cross section is made by the single reciprocal lattice point $(2, \bar{2}, 0)$ the effective polarization near the peak is [15]:

$$P_\gamma = k \left[\frac{2(1-x)}{1+(1-x)^2} \right] \frac{\beta-1}{\beta} \quad (11)$$

where $x = E_\gamma/E_0$; $\beta = (C_{\parallel}^{max} + C_{\perp}^{max})/2C_\alpha$; $C_{\parallel(\perp)}^{max}$ is the proton yield in the maximum of the orientation dependence $C_{\parallel(\perp)}$ for the two directions of the polarization vector, C_α is

the yield under the same kinematic conditions, but measured with the disoriented crystal. A coefficient k takes into account a small contribution into the coherent bremsstrahlung cross section is made by the single reciprocal lattice points of the diamond crystal next to $(2, \bar{2}, 0)$; k varies from 0.98 to 0.9 with x varying from 0.1 to 0.4. The advantage of the method for determining the polarization is connected with the fact that the presence in the reaction yields C_{\parallel}, C_{\perp} of noncoherent background (from the background reactions with $P_{\gamma}\Sigma \approx 0$) does not affect the value of asymmetry due to the taking into account of the background in the value of effective polarization.

iv) Radiation damage and heating of the crystal

To diminish radiation damage on the crystal it is proposed to use in the experiment the electron beams of 1 → 2 mm in diameter. The electron beams of these dimensions are used in experimental studies with the Kharkov linear electron accelerator for obtaining, in particular, polarized photon beams on diamond crystals with a thickness up to 2 mm ($\leq 0.015x_0$). The expertise acquired shows that the single crystal conserves its properties, until getting an integral dose of $\approx 10^{21} e^-/cm^2$, during long cycles of work with pulsed electron beams at average current up to 2.5 μA (pulsed currents of $\approx 50 mA$) without applying any special means for heat removal. Upon getting the dose, the mechanical destruction of the crystal is possible. This dose will be acquired during ≈ 50 hours of continuous running of the CEBAF accelerator at a current of 30 μA and a beam diameter of 2 mm, or during 150 hours at a current of 10 μA . Turning the crystal during the measurements around electron beam axis provided the axes of the beam and rotation are not coincide on 1-2 mm we can increase the lifetime by 3-4 times. According to the estimates of required statistics (Table 4) and measurement time (Table 5) the experiment can be performed with one crystals.

Difficulties connected with the use of high electron currents are mainly caused by the local overheating of the crystal, which can lead to the destruction of the lattice. However, these difficulties cause serious troubles only for the measurements in the energy region above 1.6 GeV, when one needs to use high electron currents of $\approx 30 \mu A$. The magnitude of power lost in the crystal at a current of 30 μA is

$$P = (dE/dx) * I * L \approx 120W$$

for the crystal with $L = 0.5$ mm ($dE/dx = 6.7$ MeV/cm for the diamond) and $P \approx 20$ W for the crystal with $L = 1$ mm. The specific power loss in case of the beam being 2 mm in diameter is ≈ 0.65 and 1.3 kW/cm², respectively.

Calculation of crystal heating shows that, under the conditions of heat equilibrium, temperature in the region of the beam (in the center of the crystal) will be by $\approx 20^\circ$ higher than at the crystal boundary, provided $I_e = 30 \mu A$, beam diameter is 0.2 cm, crystal diameter is 1 cm and the temperature of a side wall of the crystal is kept to be $20^\circ C = 293^\circ K$. This should not be difficult. Similar values ($\approx 0.5 kW/cm^2$) of specific power loss were obtained in an experiment [17] with the Darmstadt linear accelerator at an electron energy ≈ 5 MeV.

The crystal is able to withstand high pulsed current load. For example, on the Kharkov LINAC during the current cycle ($\approx 1 \mu sec$) an energy of approximately 55 kJ (≈ 800 kJ/cm²) is released in a crystal of thickness 0.2 cm, and is dissipated naturally without actively cooling the crystal during the time between the current cycles (0.02 sec). With the aim of decreasing the deposition of the heat energy in the crystal we are planning

limit the beam current the values of $\approx 30\mu A$ for 1 mm thick crystal.

v) Deuteron target

We suppose to use in the experiment the liquid deuterium 10 cm-long target being developed by California State University at Los Angeles and CEBAF [16]. This target is designed for electron beams as small as 0.1 mm in diameter, current up to $200\mu A$, and a power loss in the target up to 1 kW. The requirements to the target in this experiment are not so high because the target will irradiate with photons only.

Reaction identification

In contrast to the SLAC experiments [1,2], where the measurements were performed at the end of the bremsstrahlung spectrum, the reaction (1) yield in the experiment proposed herein should be measured in the photon region near the maximum of the coherent peak, which should be located within the relative energy range $x \leq 0.5$ for the degree of photon polarization to be high enough. Thus the conditions of the reaction identification will be essentially different. To single out the reaction (1) from the background of the competing contributions it is necessary to measure pn coincidences.

For detecting protons we propose to use the hadron spectrometer (HRS) of Hall A with its standard detectors.

To detect neutrons, it might be possible to use one of the three neutron detectors currently planned for Hall A. The neutron polarimeter of Dick Madey of Kent State for the neutron electric form factor experiment (89-005) could be used instead simply as a neutron detector. The high resolution detector planned by John Watson of Kent State would be very appropriate, especially for the higher neutron energies at which sufficient energy resolution must be maintained to eliminate events in which π production occurred. Finally the HARP collaboration plans to bring their neutron detector, which is currently under construction, to CEBAF after finishing a series of experiments at NIKHEF. We have started discussions with these groups concerning the use of their detectors for this experiment. These discussions should be complete by the time of the PAC. For now, we will assume that a new detector is needed, and describe it below.

To detect neutrons, we propose to use a hodoscope of 12 scintillation counters 20 cm thick, 10 cm wide and 16.2 cm high (hodoscope total dimensions are 30 cm in horizontal and 65 cm in vertical direction). The hodoscope is to be placed 5 m from the deuteron target center when the measurements are performed at an angle of 90° . These geometrical dimensions allow one to match the solid angles of the proton and neutron arm when detecting pn coincidences. To suppress charged particle background, scintillator counters for anticoincidences vetoes are placed in front of each neutron counter.

The neutron counter is shielded by concrete blocks. A lead absorber 10 cm thick ($17.68 X_0$) is proposed to be placed in front of the counter for decreasing the loading of the counters with charged particles and photons. With the purpose of more reliable separation of deuteron photodisintegration we propose, besides the angle, to measure neutron energy by using time of flight.

Estimates of count rate in proton and neutron arms

Estimates of the expected count rates in the proton and neutron arms under the kinematic conditions of the experiment (Table 1) are presented in Table 2. In the calculations it was assumed that:

- the solid angle of the spectrometer is $7 \mu sr$, momentum acceptance is 5% and proton

detection efficiency is 100%;

- the low-temperature liquid deuterium target is 10 cm long ($0.51 \cdot 10^{24}$ nuclei/cm²);
- the fraction of neutron passing through the 10 cm thick lead absorber is 0.57, neutron registration efficiency is 0.2;
- the thickness of the input and output aluminium window of the deuteron target is 0.1 mm;
- the photon target is the diamond single crystal of thickness 0.5 mm;
- electron beam energy is $E_0 = 4$ GeV;
- the solid angle of the neutron counter is matched to the angular acceptance of the spectrometer.

To calculate $d(\gamma,p)n$ reaction yield the number of real photons for the oriented and disoriented diamond crystal were estimated in the energy range specified by reaction kinematics and $\pm 5\%$ momentum acceptance.

The data on differential cross sections of the $d(\gamma,p)n$ reaction was taken from the SLAC experiments [1,2], and extrapolated to the regions where the data are absent (Table 1).

The differential cross sections of the background reactions due to photon interaction with the deuteron target and target walls were calculated in the standard way [18]. The number of equivalent photons was calculated for the disoriented diamond target (similar to an amorphous target of the same thickness).

Table 2 presents the results of the calculations of the yields of deuteron photodisintegration from the interaction of bremsstrahlung and coherent radiation with the deuteron target, and also the proton and pion yield in the photodisintegration of the deuteron. The expected total counting rate caused by protons and all other charged particle is presented. Since the contribution of the target walls into the total particle yield was not higher than $5 \rightarrow 10\%$, the calculation of the former are presented only for an angle of 90° .

Additional count rate in the proton arm, caused by photodisintegration in the diamond radiator target will be practically absent, because the spectrometer does not "see" the photon target. Additional line of sight neutron shielding may be required for the spectrometer detector. Count rate in the neutron arm for crystals 0.5-1 mm thick will increase approximately on 10-15%. However, to decrease the count rate we propose to use concrete shielding wall ≈ 1 m thick, which is placed near the goniometer. The wall will allow one to almost completely get rid of the background from the photon target in the neutron detector.

The expected count rate of protons in proton arm does not exceed 10^4 sec⁻¹. Under these conditions the detection system will be able, with high efficiency, to suppress the background of pions, positrons and other charged particles.

The count rate of the counters of the neutron telescope includes the neutrons as well as the charged particles. To estimate the counting rate, the calculated spectral distributions of protons, pions and neutrons were integrated over particle momentum in the range from 50 to 1700 MeV/c, taking into account particle absorption in the lead absorber and neutron detection efficiency. In Table 3 the results of count rate calculations are shown. The target wall contribution is small and was not taken into account. The charged pions are the main contribution into the count rate of the neutron counter. The neutron count rate is lower by an order of magnitude. Since the total count rate of each neutron counter of the hodoscope does not exceed 10^5 sec⁻¹ suitable electronic with a time resolution of $10^{-8} \rightarrow 10^{-9}$ sec will ensure efficient suppression of the charged particle background.

Count rate of proton neutron coincidences

The count rate of pn coincidences was calculated in an assumption of a match of the solid angles of the proton and neutron arm. The absorption of neutrons by the lead absorber and neutron detection efficiency were taken into account in the calculations. The yield for the oriented ($d(\gamma,p)n$ cryst.) and disoriented ($d(\gamma,p)n$ amorph.) crystal were calculated. The results are presented in Table 4. The magnitude of the accidental coincidences was estimated from the total count rate in the proton (total p, amorph.) and neutron (total n) arm with resolution time of the coincidence assumed to be $\approx 2 * 10^{-9}$ sec.

Required statistic and beam time for the experiment

If one neglects the contribution of background pn coincidences from the target walls, the experiment proposed herein implies that the measurements of the yield of pn coincidences should be performed under the following conditions:

- when the polarization vector is parallel (C_{\parallel}) or perpendicular (C_{\perp}) to the reaction plane;
- when the crystal is disoriented (C_a).

The asymmetry is determined by the following expression:

$$\Sigma = \frac{1}{P_{\gamma}} \frac{C_{\parallel} - C_{\perp}}{C_{\parallel} + C_{\perp}} \quad (12)$$

The polarization magnitude P_{γ} is calculated in accordance with (11) by using data on the C_{\parallel} , C_{\perp} and C_a yields which have been measured.

The statistics for $C_{\parallel} + C_{\perp}$ and C_a for ensuring the required precision for the asymmetry $\Delta\Sigma$ measurement is shown in Table 4. Time requirements were estimated with the use of values of $C_{\parallel} + C_{\perp}$ and C_a and the corresponding count rates of pn coincidences (which are presented in Table 4). The estimates were performed with the use of the calculated values of photon beam polarization; the asymmetry value for $E_{\gamma} \leq 1$ GeV and $\theta_p^{cm} = 90^{\circ}$ were taken from [14], while for other experimental conditions they were considered to be at a level of $\Sigma = 0.15$. It should be noted that the required statistics are weakly dependent on the asymmetry magnitude.

Time for gaining the required statistics for crystal 0.5 mm thick is estimated to be 198 hours. Time for measurements at angles of 60° and 120° for getting angular distributions at 1.0, 1.4 and 2 GeV is ≈ 50 hours. The total time for gaining statistics is ≈ 248 hours. The total time for running the experiment is presented in Table 5.

The total time for the experiment

Running the experiment also requires additional beam time:

- 50 hours for the calibration of equipment and test measurement;
- 50 hours for performing crystal orientation, and changing the energy of the interference maximum (coherent peak energy), angles and spectrometer magnetic field;
- 50 hours for measurements with the empty target.

The total time of the experiment with crystals of different thickness is shown in Table 5. This time is 398 hours for 0.5 mm thick crystal and 273 hours for 1 mm thick crystal.

At the first stage of the experiment one may restrict oneself by measuring only two energy dependencies of the asymmetry (for angles of 30° and 90°) and three angular distributions. In this case the total time for the experiment is ≈ 250 hours and ≈ 190 hours with the crystal of thickness 0.5 mm and 1 mm, respectively.

The experiment results expected are presented in Fig. 5.

Tests and reliability of the experimental procedure

The accuracy of the proposed procedure for the asymmetry measurement is confirmed by the results of recent measurements of the asymmetry of the $\gamma d \rightarrow pn$ and $\gamma p \rightarrow p\pi^0$ reaction performed in Brookhaven [19] with a linear polarized photon beam produced as a result of the Compton scattering of laser radiation on relativistic electrons (Fig.10). The data obtained in these experiments are in good agreement with the data [15,20,21] obtained with the proposed procedure in Kharkov.

Collaboration

The experiment proposed may be considered as part of the experimental program for studying the deuteron photodisintegration process in Hall A. The main part of the experiment may be carried out simultaneously with the measurements of proton polarization in the same reaction [8].

The KhPTI can take upon itself work on obtaining the polarized photon beam, developing the magnetic system for the separation of the electron and photon beam in Hall A, producing single crystal targets and their preliminary orientation with the KhPTI linear accelerator and studying the radiation resistance of the crystals at high electron currents. KhPTI can also take upon itself work (or a part of work) on the construction of the neutron detector, if required.

CONCLUSIONS

We have been studied the possibility to investigate the $\gamma d \rightarrow pn$ reaction with CLAS detector.

1) If CLAS detector is operated in the ordinary mode with the tagged photon beam intensity 10^7 sec^{-1} and charged hadron trigger then the beam time is required 10^2 larger than for proposed variant.

2) If CLAS detector is operated without tagged photons and with charged hadron-neutron coincidences trigger then:

- in these case there is no start signal for the time of flight measurements and it will be very difficult to organize it by inner detector in CLAS at intensity of $\approx 10^9 \gamma/\text{sec}$;

- neutron detector (calorimeter) cannot measure the neutron angle with good efficiency. So the $\gamma d \rightarrow np$ events reconstruction has many problem in these conditions.

- measurements can be done at the 30-70 deg. c.m.s. angles only.

Moreover, CLAS probably can not operate properly at photon flux $\approx 10^9 \rightarrow 10^{10} \gamma/\text{sec}$ with deuteron target which is planned to use in the experiment ($N=0.51 \cdot 10^{24} \text{ nuclei/cm}^2$) because CLAS maximum luminosity is $\approx 10^{34} \text{ cm}^{-2} \cdot \text{sec}^{-1}$. So at today level of design of CLAS performance, it is not possible to do the experiment on $\gamma d \rightarrow pn$ at $E_\gamma \geq 1.2-1.4 \text{ GeV}$ with CLAS detector.

The cost of the magnet by pass system and shielding is about 30-40 k\$ what is not expensive. We can use the CEBAF C-dipole magnets which cost about 10 k\$ each.

So it is quite reasonable to construct this by-pass magnetic system at Hall A especially taking into account that the system could be used in many other experiments which require

an intense photon beam. And this by-pass system is quite necessary for measurements at more high photon energies E_γ up to 3-3.5 GeV which will become available if maximum electron energy at CEBAF will be increase up to 6 GeV.

It should also be noted that if the experiment is implemented, the system developed provides prospective possibilities of performing a wide range of experiments with photon beams for which high luminosity is required, and, in particular, it will essentially simplify and reduce the time requirements and systematic uncertainties of the experiment for the measurement of the polarized proton [8].

REFERENCES

1. J.Napolitano et. al., Phys. Rev. Lett. 61, 2530 (1988).
2. D.H.Potterveld, (1992).
3. V.A.Matveev, R.M.Muradyan, A.V.Tavkhelidze, Lett. Nuovo Cim. 7, 719, (1973).
4. S.J.Brodsky, G.R.Farrar, Phys. Rev. Lett. 31, 1153 (1973).
5. S.J.Brodsky, G.R.Farrar, Phys. Rev. D11, 1309 (1975).
6. S.J.Brodsky, J.R.Hiller, Phys. Rev. C28, 475 (1983).
7. CEBAF proposal 89-012 (1989).
8. CEBAF proposal 89-019 (1989).
- 9.S.I.Nagornij, Ju.A.Kasatkin, I.K.Kirichenko, Nucl. Phys.(russian),55, 345,(1992).
10. T.S.H.Lee, Proceedings of the International Conference on Medium and High-Energy Nuclear Physics, Taipei, Taiwan, 23-27 May 1988.
11. Y.Kang et. al., Program of the Particles and Nuclei Conference, MIT, Cambridge, MA., p.1-40, 1990.
12. F.Gross, B.D.Keister, Phys. Rev. C28, 823 (1983).
13. Y.Burkert et.al., Deuteron Photodisintegration. Letter of Intent for the CEBAF project, 1988.
14. F.V.Adamian et. al., J. Phys. C: Nucl. Phys. 17, 1657 (1991).
15. V.G.Gorbenko et. al., Nucl. Phys.(russian),35,1073 (1982).
16. C.S.Sapp, A.Saha, Report CEBAF, (1990).
17. W.Lotz et.al., Nucl.Inst.and Meth. B48, 256, (1990).
18. J.W.Lightbody et.al., Computers in Physics, May/June, p.57 (1988).
19. LEGS Progress Report (June 92).
20. V.B.Ganenko et. al., Nucl. Phys., 23, 162 (1976).
21. A.A.Beljaev et. al.,Nucl. Phys., 35, 401 (1982).

Table 1. Kinematics for the measurements.

$$\theta_p^{cm} = 30^\circ$$

E_γ GeV	θ_p^{lab} deg	P_p GeV/c	T_p GeV	$(d\sigma/d\Theta)_D^{lab}$ nb/sr
0.6	21.1	1.038	0.461	837
0.8	20.1	1.261	0.634	309
1.0	19.1	1.475	0.81	135
1.2	18.4	1.682	0.988	57.7
1.4	17.7	1.885	1.168	27.3
1.6	17.1	2.068	1.349	17.5
1.8	16.5	2.284	1.531	12.5
2.0	16.0	2.48	1.713	6.6
2.2	15.6	2.675	1.896	4.2
2.4	15.2	2.869	2.08	3.0

$$\theta_p^{cm} = 90^\circ$$

E_γ GeV	θ_p^{lab} deg	P_p GeV/c	T_p GeV	$(d\sigma/d\Theta)_D^{lab}$ nb/sr
0.6	68.2	0.806	0.299	660
0.8	65.2	0.953	0.399	228
1.0	62.7	1.089	0.499	80
1.2	60.5	1.218	0.599	21
1.4	58.6	1.342	0.699	8.3
1.6	56.8	1.462	0.799	3.0
1.8	55.3	1.58	0.899	1.6
2.0	53.9	1.695	0.999	0.81
2.2	52.5	1.808	1.099	0.4
2.4	51.3	1.92	1.199	0.21

$$\theta_p^{cm} = 150^\circ$$

E_γ GeV	θ_p^{lab} deg	P_p GeV/c	T_p GeV	$(d\sigma/d\Theta)_D^{lab}$ nb/sr
0.6	134.5	0.525	0.137	152
0.8	131.7	0.579	0.164	46.3
1.0	129.1	0.624	0.188	13.9
1.2	126.8	0.662	0.21	7.8
1.4	124.7	0.697	0.23	3.52
1.6	122.8	0.728	0.249	1.77
1.8	121.0	0.757	0.268	0.8
2.0	119.3	0.785	0.285	0.38
2.2	117.2	0.811	0.302	0.2
2.4	116.2	0.836	0.31	0.1

Table 2. Count rates in the proton arm.
 $\theta_p^{cm} = 90^\circ$, for Al targets walls

E_γ GeV	I_e μa	$(\gamma,p)X$ sec^{-1}	$(\gamma,\pi)X$ sec^{-1}	total($\pi+p$) sec^{-1}
0.6	1	0.13	0.10	0.23
0.8	1	0.04	0.03	0.07
1.0	3	0.05	0.02	0.07
1.2	6	0.04	0.01	0.04
1.4	10	0.04	-	0.04
1.6	20	0.03	-	0.03
1.8	30	0.03	-	0.03
2.0	30	0.02	-	0.02

$\theta_p^{cm} = 90^\circ$, for deuterium

E_γ Gev	I_e μA	$d(\gamma,p)n$ amorp sec^{-1}	$d(\gamma,p)n$ crystal sec^{-1}	$d(\gamma,p)X$ amorp sec^{-1}	$d(\gamma,\pi)X$ amorp sec^{-1}	total amorp sec^{-1}	total amorp sec^{-1}	total crystal sec^{-1}
0.6	1	5.67	28.1	-	6.67	12.34	5.67	28.3
0.8	1	1.92	7.86	-	1.75	3.67	1.92	7.86
1.0	3	1.92	6.46	-	1.25	3.17	1.92	6.46
1.2	6	1.00	2.85	-	0.08	1.08	1.00	2.85
1.4	10	1.11	2.53	-	-	1.11	1.11	2.53
1.6	20	0.56	1.11	-	-	0.56	0.56	1.11
1.8	30	0.44	0.83	-	-	0.44	0.44	0.83
2.0	30	0.21	0.37	-	-	0.21	0.21	0.37
2.2	30	0.10	0.17	-	-	0.10	0.10	0.17
2.4	30	0.05	0.08	-	-	0.05	0.05	0.08

$\theta_p^{cm} = 30^\circ$, for deuterium

E_γ Gev	I_e μA	$d(\gamma,p)n$ amorp sec^{-1}	$d(\gamma,p)n$ crystal sec^{-1}	$d(\gamma,p)X$ amorp sec^{-1}	$d(\gamma,\pi)X$ amorp sec^{-1}	total amorp sec^{-1}	total amorp sec^{-1}	total crystal sec^{-1}
0.6	1	7.75	38.8	483	958	1449	491	522
0.8	1	2.58	10.6	383	675	1061	386	394
1.0	3	3.25	10.9	875	1475	2353	878	886
1.2	4	1.67	4.76	867	1367	2236	869	872
1.4	10	2.08	4.74	1583	2396	3981	1585	1588
1.6	10	1.33	2.66	1150	1650	2801	1151	1153
1.8	15	1.25	2.35	1250	1700	2951	1251	1252
2.0	20	1.00	1.75	1167	1500	2268	1168	1169
2.2	30	1.00	1.67	1400	1650	3051	1401	1402
2.4	30	0.61	0.97	915	1230	2146	916	916

$\theta_p^{cm} = 150^\circ$, for deuterium

E_γ Gev	I_e μA	d(γ, p)n amorp sec ⁻¹	d(γ, p)n crystal sec ⁻¹	d(γ, p)X amorp sec ⁻¹	d(γ, π)X amorp sec ⁻¹	total amorp sec ⁻¹	total amorp sec ⁻¹	total crystal sec ⁻¹
0.6	1	1.32	6.58	-	-	1.32	1.32	6.58
0.8	1	1.14	4.67	-	-	1.14	1.14	4.67
1.0	3	0.55	1.85	-	-	0.55	0.55	1.85
1.2	5	0.58	1.67	-	-	0.58	0.58	1.67
1.4	10	0.50	1.14	-	-	0.50	0.50	1.14
1.6	20	0.36	0.72	-	-	0.36	0.36	0.72
1.8	30	0.18	0.34	-	-	0.18	0.18	0.34
2.0	30	0.08	0.14	-	-	0.08	0.08	0.14

Table 3. Counting rates for one counter in the neutron arm.

θ_p^{cm} deg	θ_n^{Lab} deg	I_e μA	d(γ, p)X sec ⁻¹	d(γ, π)X sec ⁻¹	d(γ, n)X sec ⁻¹	total p, π , n sec ⁻¹	total n sec ⁻¹
30	133.5	1	-	254	17	271	17
60	98.2	1	0.04	126	15	141	15
90	68.2	1	1.05	160	13	173	13
90	53.9	1	19	376	24	419	24
120	44.9	1	33	366	15	414	15
150	21.2	1	129	822	28	979	28

Table 4. Count rates for pn coincidences on deuterium.

$\theta_p^{cm} = 30^\circ$

E_γ GeV	I_e μA	P_γ	$\Delta\Sigma$	d(γ, p)n amorp sec ⁻¹	d(γ, p)n crystal sec ⁻¹	$C_{ } + C_{\perp}$ counts	C_a counts	accid trues %	T hours
0.6	1	0.74	0.05	0.88	4.42	974	642	0.06	0.26
0.8	1	0.70	0.05	0.29	1.21	1090	640	0.15	0.86
1.0	3	0.67	0.05	0.37	1.24	1216	662	0.81	0.77
1.2	4	0.62	0.05	0.19	0.54	1389	658	2.12	1.68
1.4	10	0.56	0.05	0.24	0.54	1702	662	8.50	1.64
1.6	10	0.49	0.05	0.15	0.30	2220	664	9.86	3.29
1.8	15	0.42	0.05	0.14	0.27	3025	673	14.7	4.45
2.0	20	0.36	0.05	0.11	0.20	4117	679	18.8	7.43
2.2	30	0.28	0.05	0.11	0.19	5929	690	34.8	10.41
2.4	30	0.22	0.10	0.07	0.11	2135	172	34.2	6.07
									total 36.86

$$\theta_p^{cm} = 90^\circ$$

E_γ GeV	I_e μA	P_γ	$\Delta\Sigma$	d(γ,p)n amorp sec ⁻¹	d(γ,p)n crystal sec ⁻¹	$C_{ } + C_{\perp}$ counts	C_a counts	accid trues %	T hours
0.6	1	0.74	0.05	0.65	3.23	974	642	0.001	0.36
0.8	1	0.70	0.05	0.22	0.90	1090	640	0.001	1.14
1.0	3	0.67	0.05	0.22	0.74	1216	662	0.003	1.29
1.2	6	0.62	0.05	0.11	0.33	1389	658	0.006	2.83
1.4	10	0.56	0.05	0.13	0.29	1702	662	0.010	3.04
1.6	20	0.49	0.05	0.064	0.13	2220	664	0.020	7.63
1.8	30	0.42	0.05	0.05	0.095	3025	673	0.03	12.58
2.0	30	0.36	0.07	0.024	0.042	2058	340	0.03	17.55
2.2	30	0.28	0.10	0.011	0.019	1482	171	0.032	25.98
2.4	30	0.22	0.20	0.006	0.010	516	103	?????	26.75
									total 99.15

$$\theta_p^{cm} = 150^\circ$$

E_γ GeV	I_e μA	P_γ	$\Delta\Sigma$	d(γ,p)n amorp sec ⁻¹	d(γ,p)n crystal sec ⁻¹	$C_{ } + C_{\perp}$ counts	C_a counts	accid trues %	T hours
0.6	1	0.74	0.05	0.15	0.75	974	642	0.001	1.55
0.8	3	0.70	0.05	0.13	0.53	1090	640	0.003	1.94
1.0	5	0.67	0.05	0.063	0.21	1216	662	0.005	4.53
1.2	10	0.62	0.05	0.066	0.19	1389	658	0.012	4.80
1.4	20	0.56	0.05	0.057	0.13	1702	662	0.024	6.86
1.6	30	0.49	0.05	0.041	0.082	2220	664	0.036	12.02
1.8	30	0.42	0.10	0.021	0.039	756	168	0.036	7.61
2.0	30	0.36	0.10	0.01	0.016	1029	170	0.035	22.59
									total 61.90

Table 5. Total time of the experiment.

Separate γ and e^- beams

Crystal thick 0.5 mm

Total time of the experiment 398 hours

Angle c.m.	Energy, GeV	I_e , μA	T, hours
30°	0.6-2.4	1-30	87
90°	0.6-2.4	1-30	149
150°	0.6-2.0	1-30	112
60°, 120°	1.0, 1.4, 2.0	1-30	50

Crystal thick 1.0 mm

Total time of the experiment 273 hours

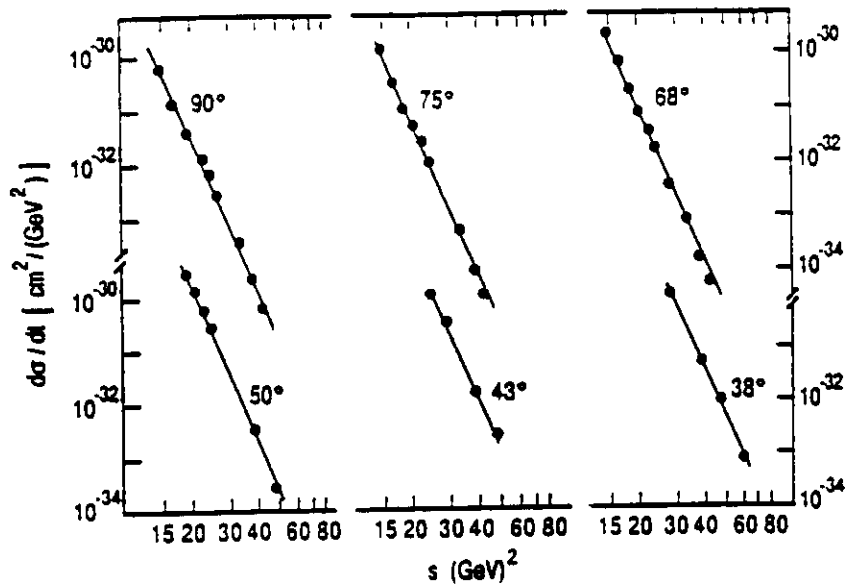


Fig. 1a. Elastic proton-proton scattering cross section, plotted versus the Mandelstam variable s , for fixed center-of-mass angles

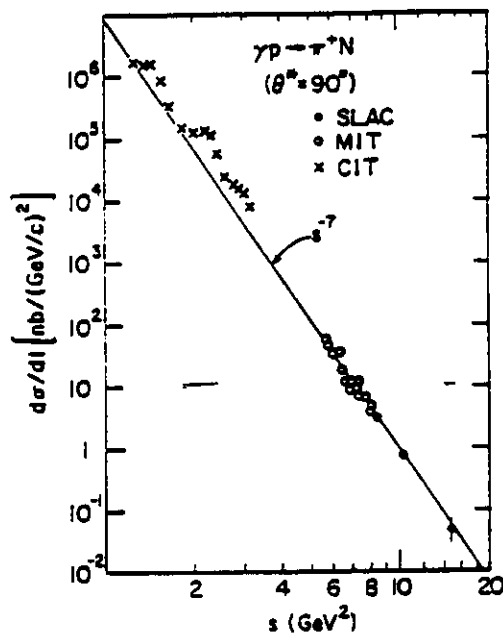


Fig. 1b. The cross section for the reaction $\gamma p \rightarrow \pi^+ n$ at a fixed center-of-mass angle as a function of the total energy squared s .

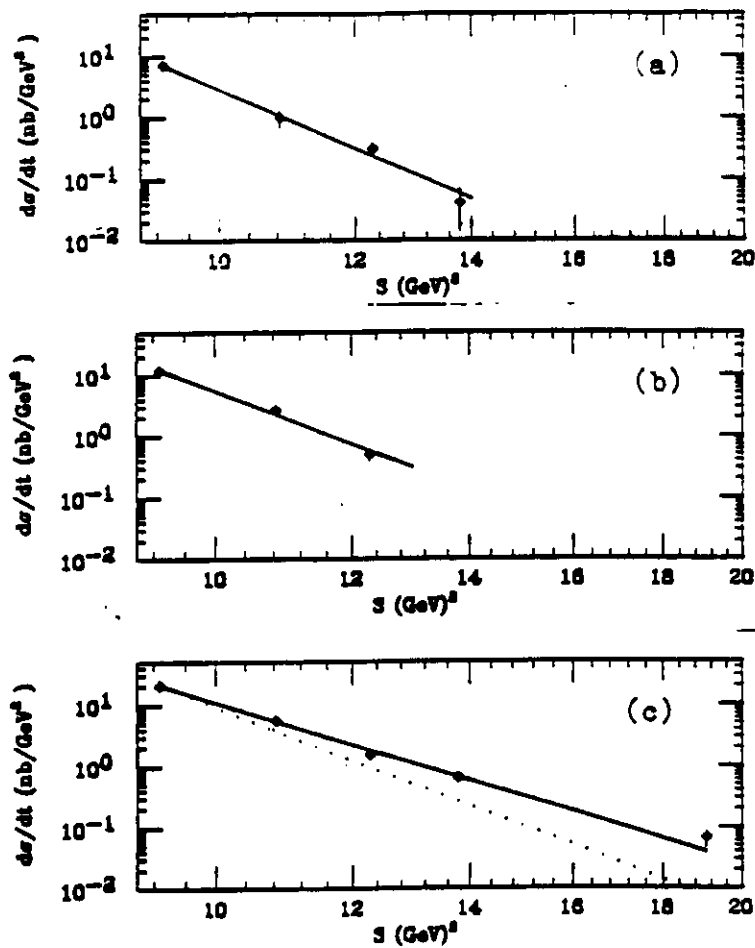


Fig. 2. Preliminary cross section data [2] for the reaction $\gamma d \rightarrow pn$ for angles 90° (a), 53° (b) and 37°. The lines are a fit to the data of the form $1/s^n$, in which $n=12.1 \pm 0.8$ (a), 11.0 ± 0.5 (b) and 8.7 ± 0.3 (c) s^{-11} extrapolation on fig.2c is plotted as the dotted line (Fig. from ref. [2]).

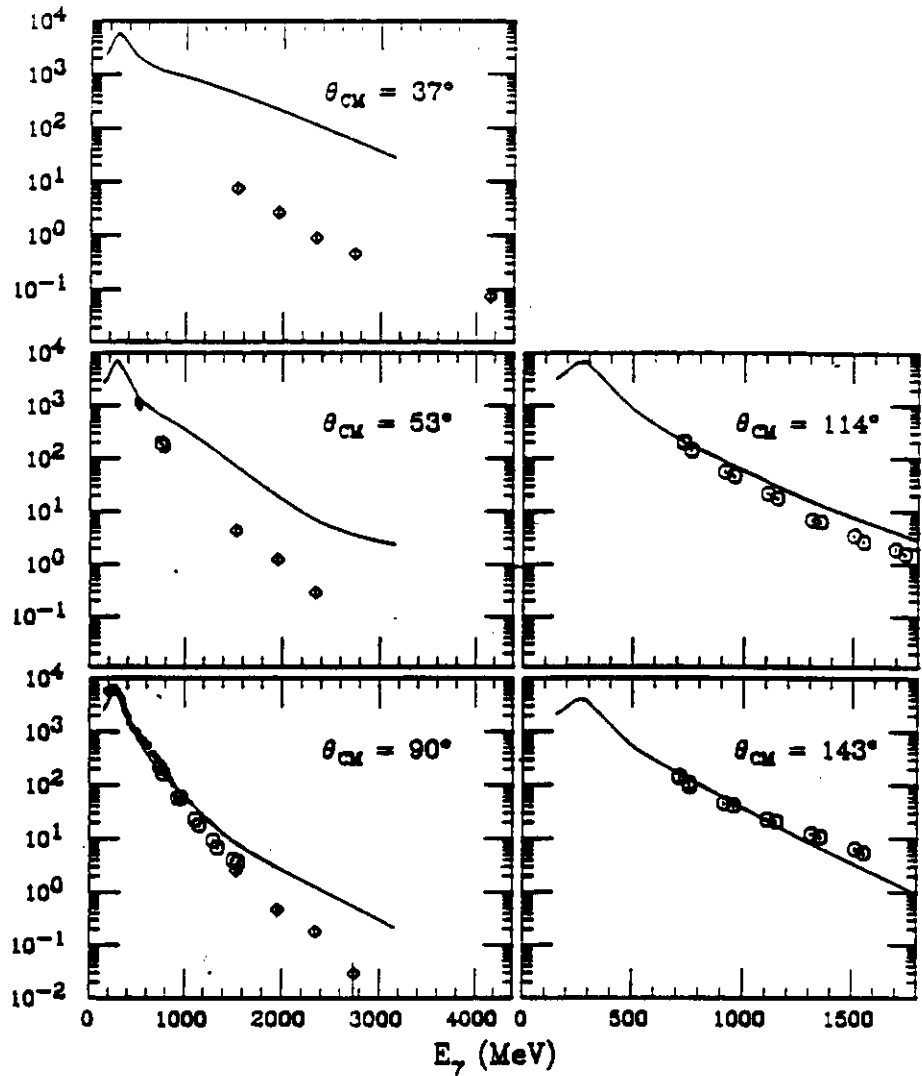


Fig. 3. $d\sigma/d\Omega^{cm}$ deuteron photoisintegration cross section in nb/sr for [1] (circles) and preliminary results [2] (diamonds). The other data points are from [24-26]. The curves are the calculations [10] for the Paris potential. (Fig. from ref.[2]).

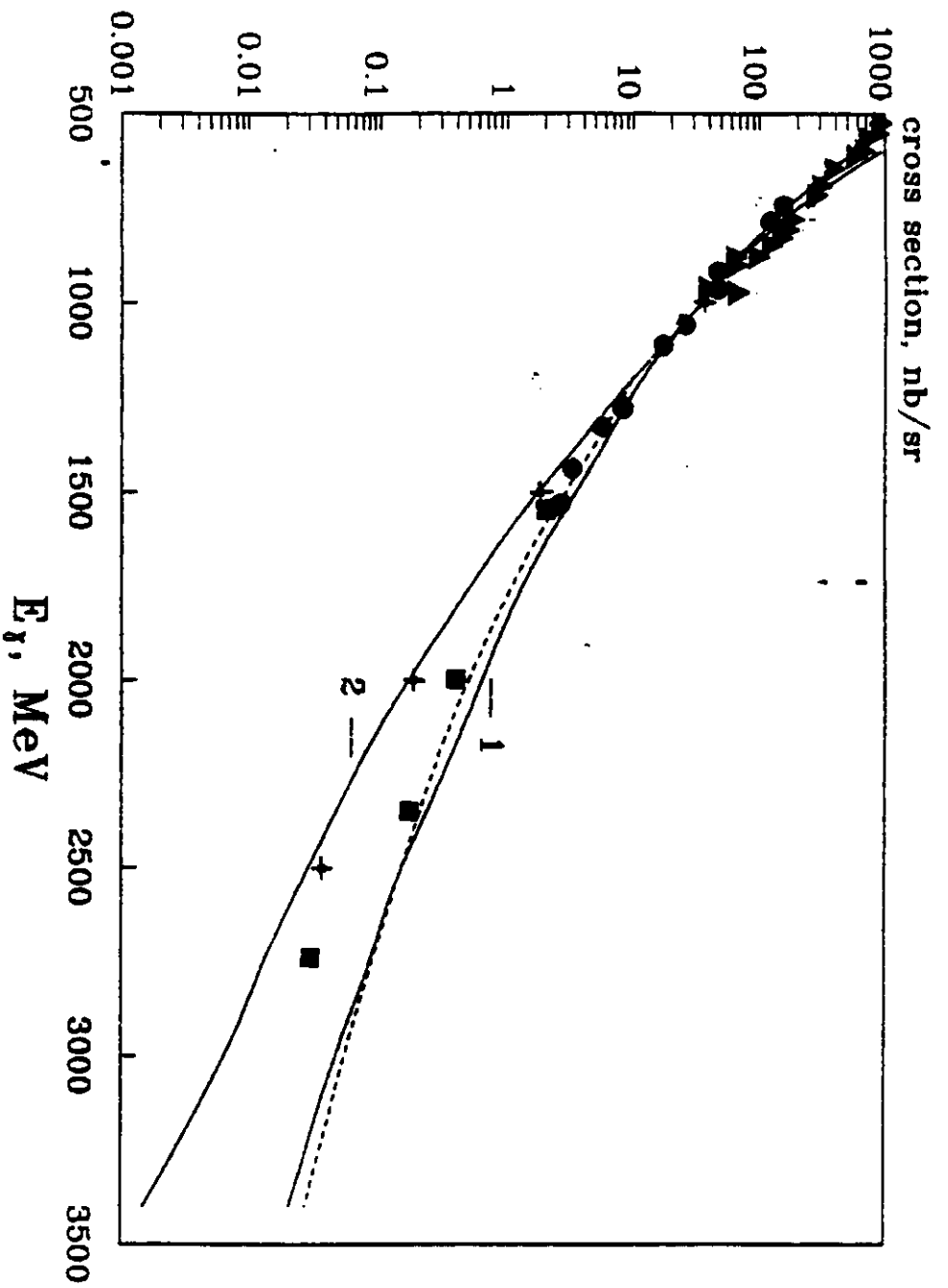


Fig. 4a. Deuteron photodisintegration cross section at a center-of-mass angle of 90° . The data are from ref.[26] (\blacktriangle), [1] (\bullet) and preliminary data from ref.[2] (\blacksquare). The curves are a calculation [9] for $\alpha=3$ (1) and $\alpha=4$ (2) when only NN configurations ($\alpha=0$) are taken into account, the dashed curve is the calculation [9] with NN and NN' configurations ($\alpha=15$) in the deuteron wave function. Crosses (+) is the results of the calculation [13] based on model [6].

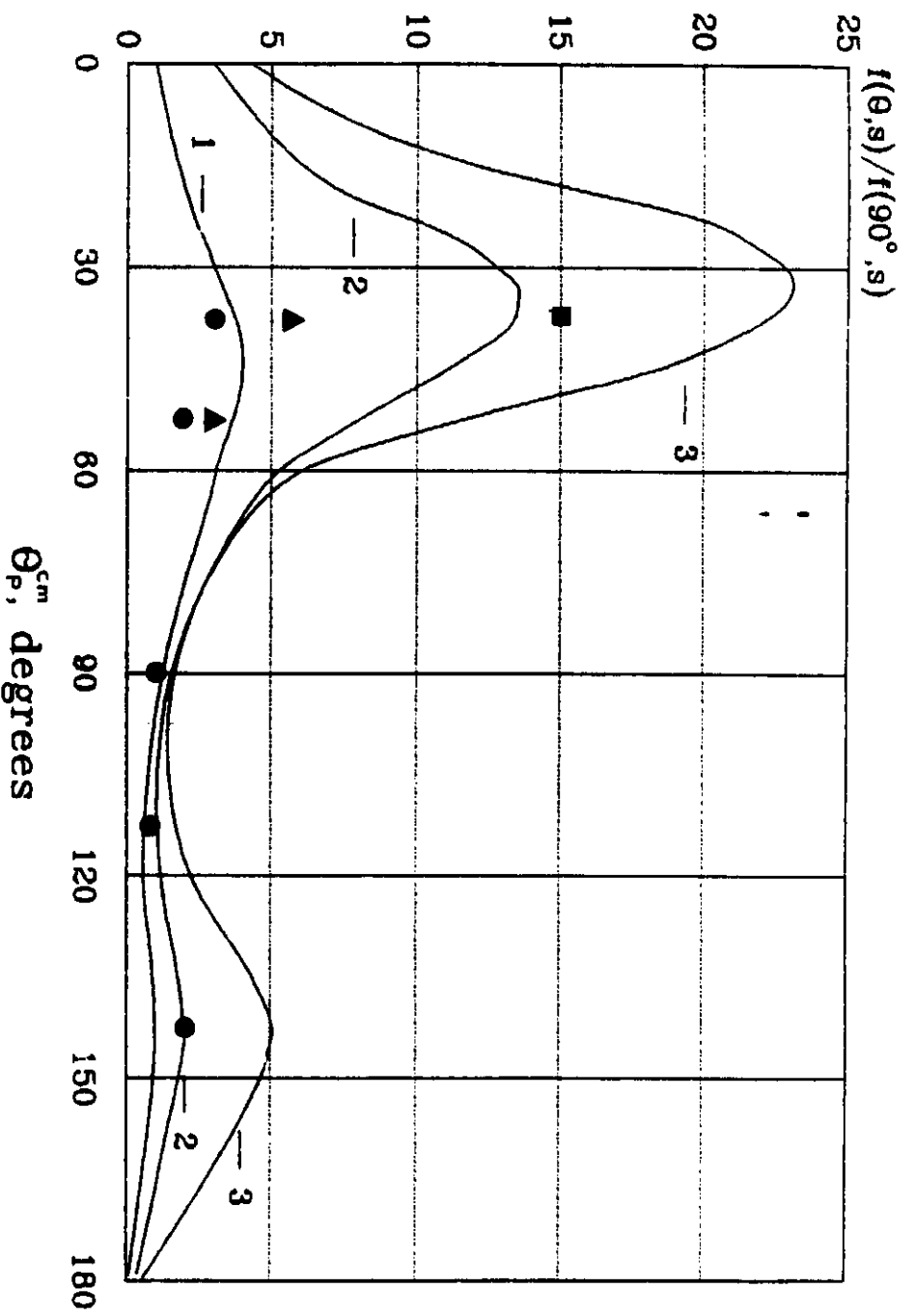


Fig. 4b. Relative angular distributions of deuteron photodisintegration. Curves are the calculation [9] for proton energies 1 GeV (1), 2 GeV (2) and 3 GeV (3) with only NN configuration in the deuteron wave function. Experimental data are from ref. [1,2] for photon energies 1.5 GeV (○), 2 GeV (▲) and 2.74 GeV (■)

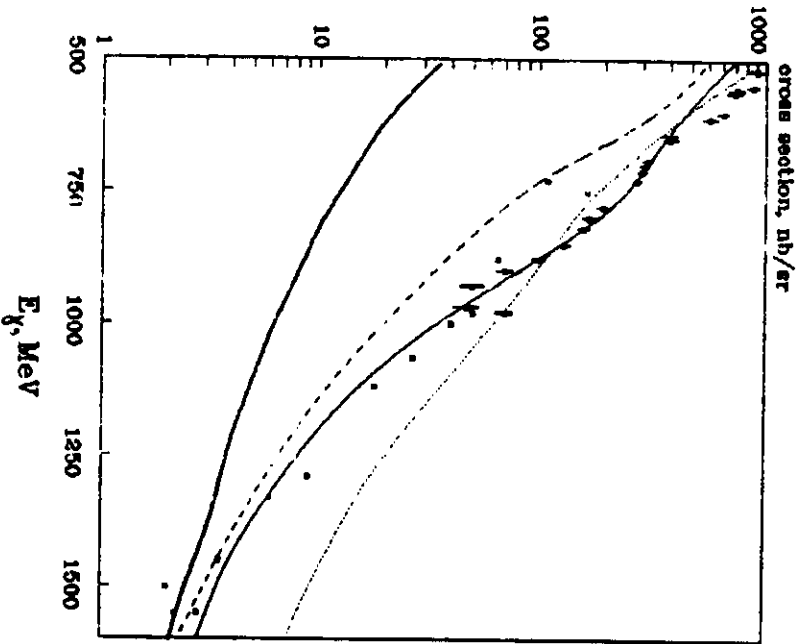


Fig.4c

Deuteron photodisintegration cross section at a center-of-mass angle 90° from ref.[11]. The curves are a calculation [11]: ——— total, ——— background(BG), - - - - BG+delta. Lee [10].

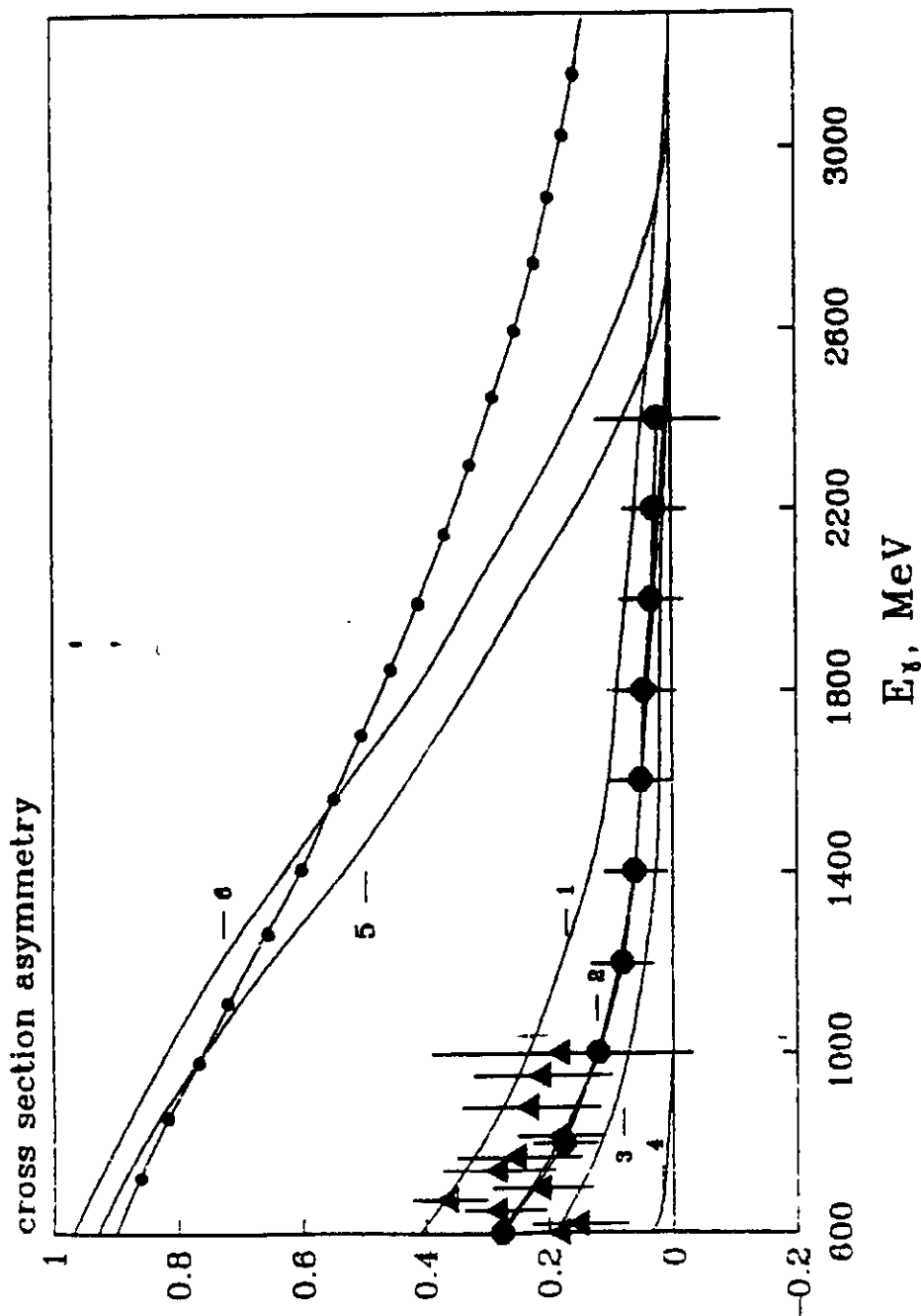


Fig. 5a. Energy dependence of the cross section asymmetry at center-of-mass angle 90° and $\alpha=3$. The curves are a calculation [9] with NN configuration ($\alpha=0$) in the deuteron wave function ($\rightarrow\bullet\rightarrow$) and when the NN^* configuration taken into account with $\alpha=10, 15, 20$ and 30 (lines 1, 2, 3, 4 respectively). Curves 5 and 6 are the off shell calculation only with NN configuration. Data from ref. [14] (Δ) circles are the respected results for proposed experiment.

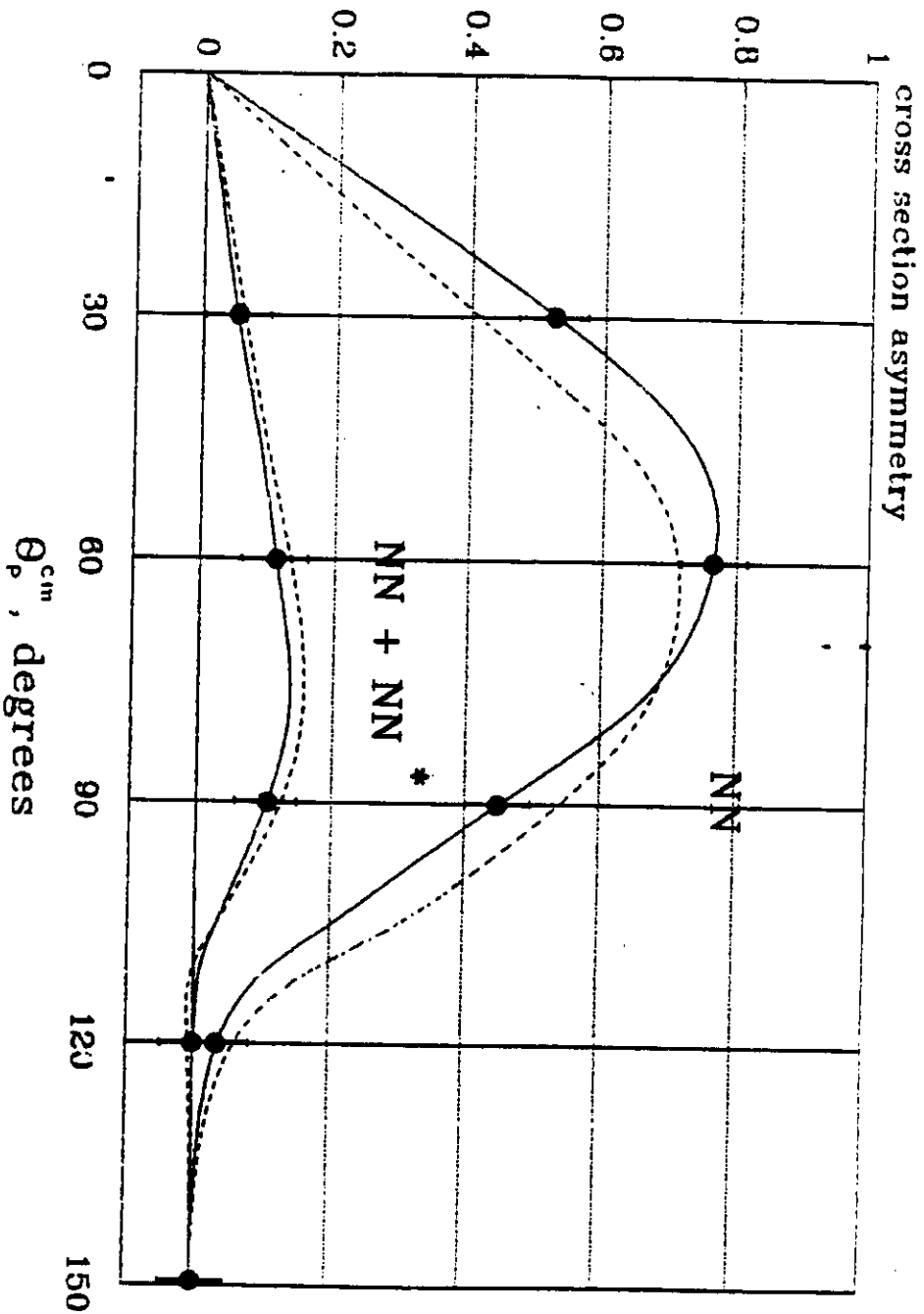


Fig. 5b. Angular distribution of the cross section asymmetry of deuteron photodisintegration for $E_\gamma=1.5$ GeV. The curves are off shell (—) and on shell (---) calculation [9] when only NN ($\alpha=0$) and NN and NN* ($\alpha=10$) configurations are taken into account in the deuteron wave function. Circles are the expectable results of the proposed experiment.

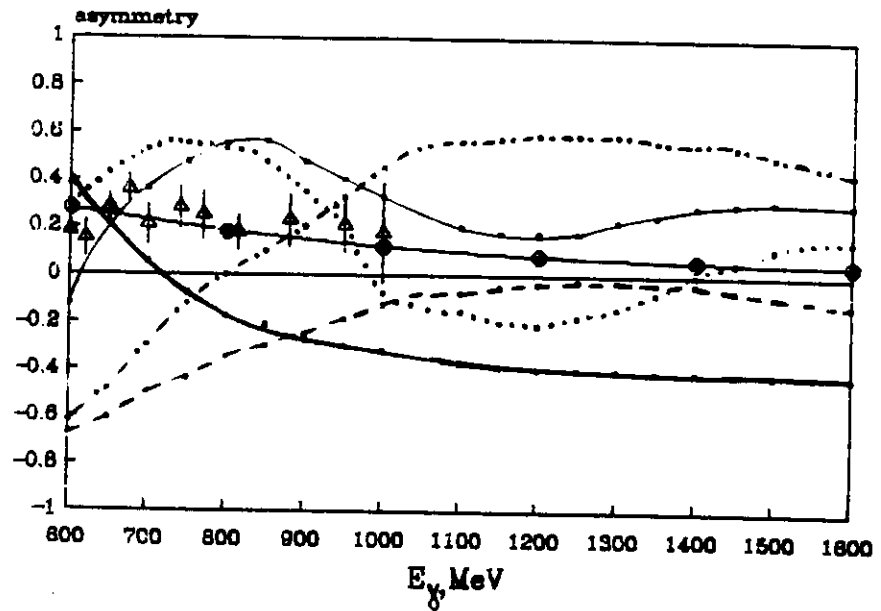


Fig.5c

Energy dependence of the cross section asymmetry at center-of-mass angle 90° . The curves are calculations [11]: _____ total, _____ background (BG), - - - - - BG+ Δ , - . - . - without D_{33} , - - - - - without D_{13} , and calculations [9] (notations see on Fig.5a). Δ - data from ref [14], circles are the respected results for proposed experiment.

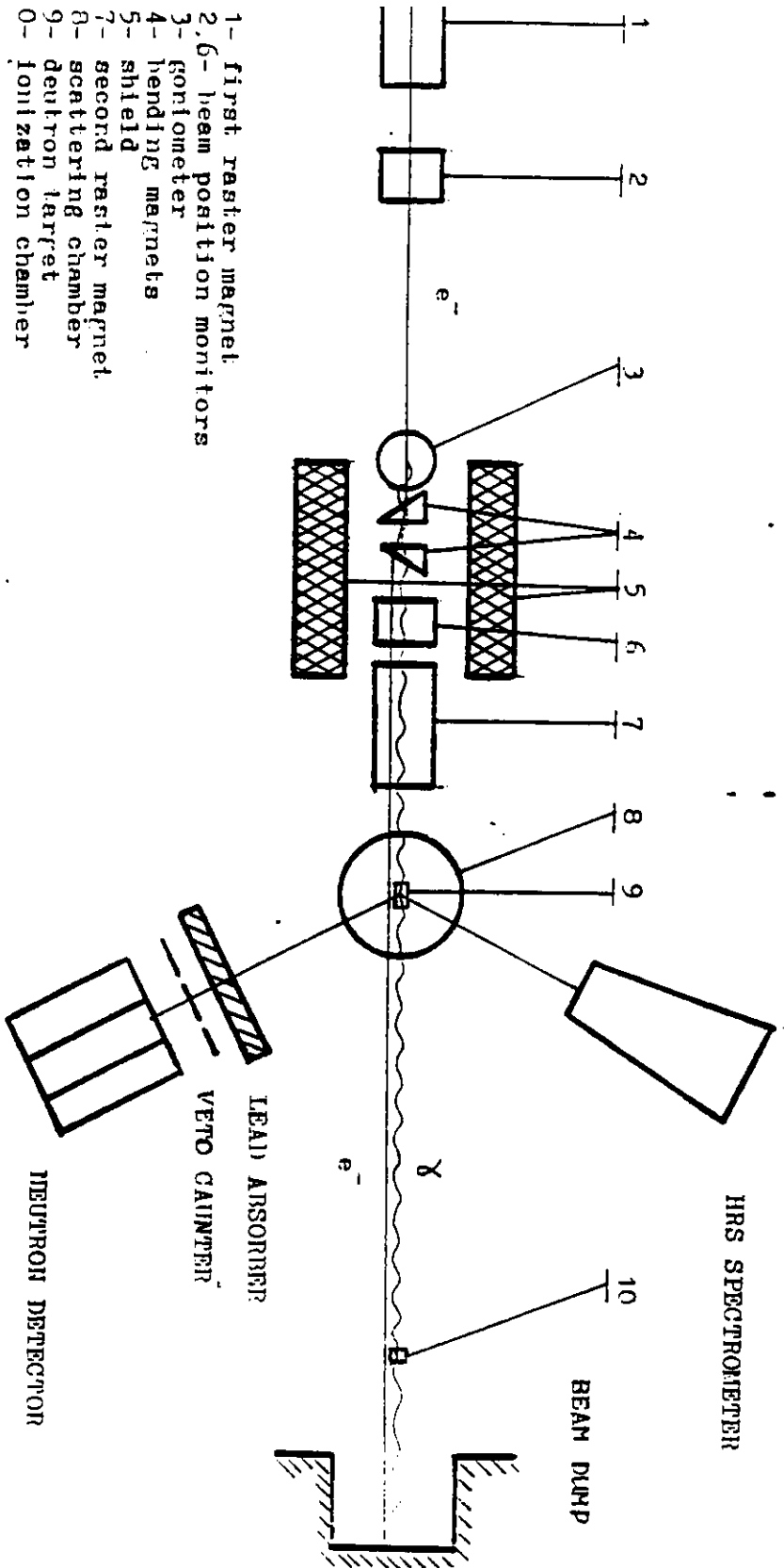


Fig. 6 Experimental set up

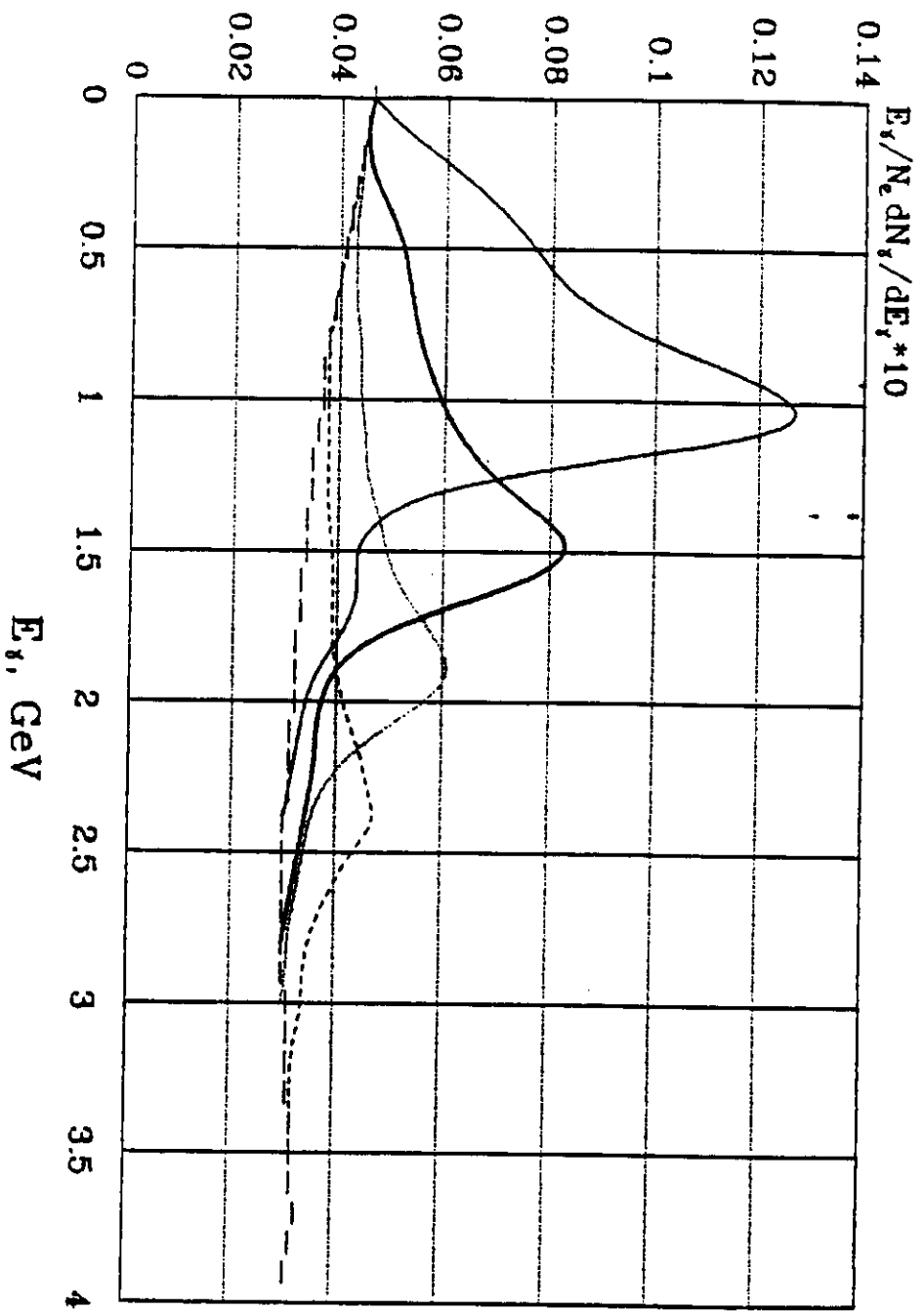


Fig. 7a Spectra of coherent bremsstrahlung for electron energy $E_p=4$ GeV and peak photon energies 1.1 GeV (—), 1.5 GeV (—), 2 GeV (.....) and 2.4 GeV. Diamond, orientation (2,2,0), thick 0.5 mmf (---) bremsstrahlung spectrum.

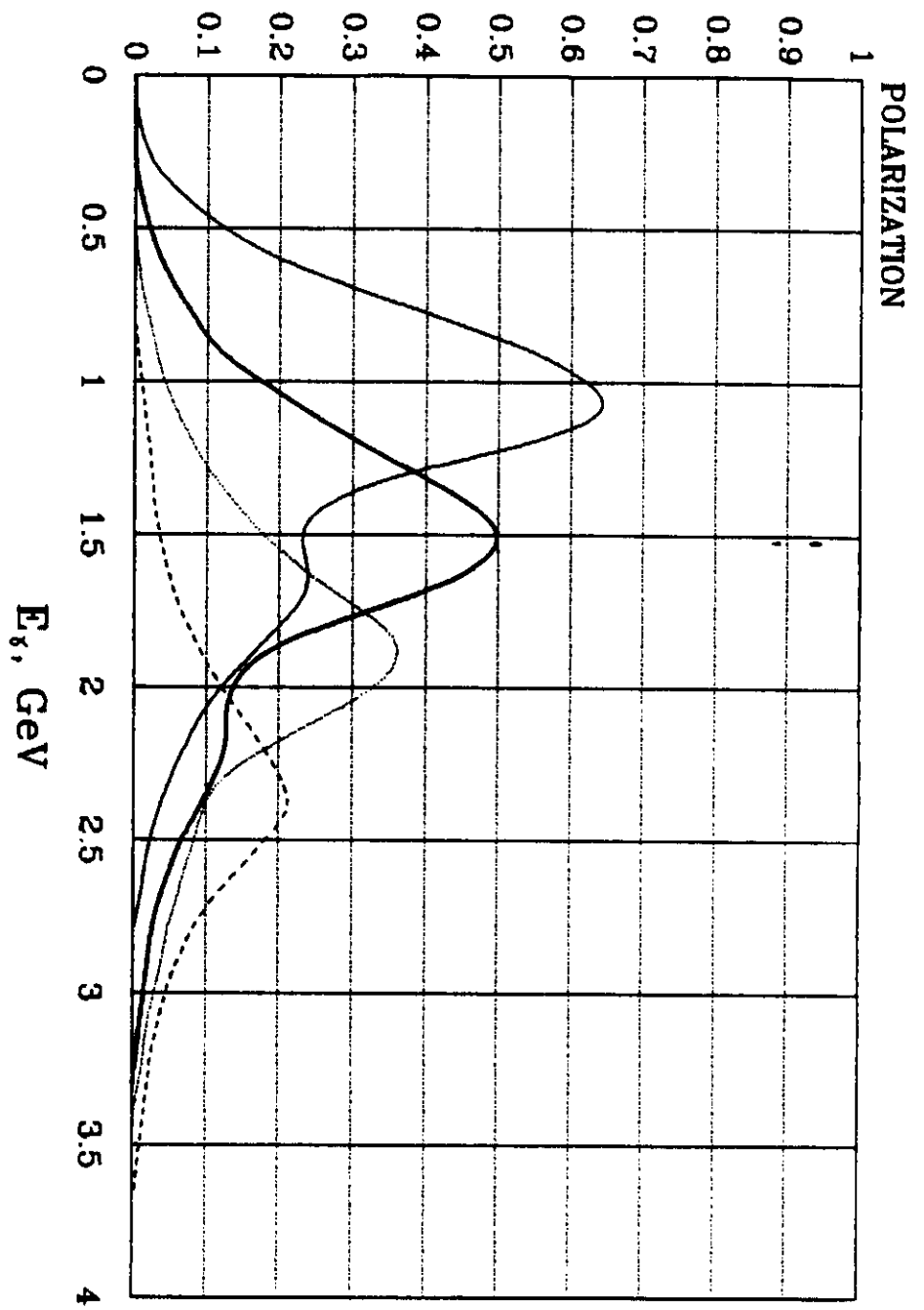


Fig. 7 b Polarization of coherent bremsstrahlung. Notation and conditions the same as in fig.7c

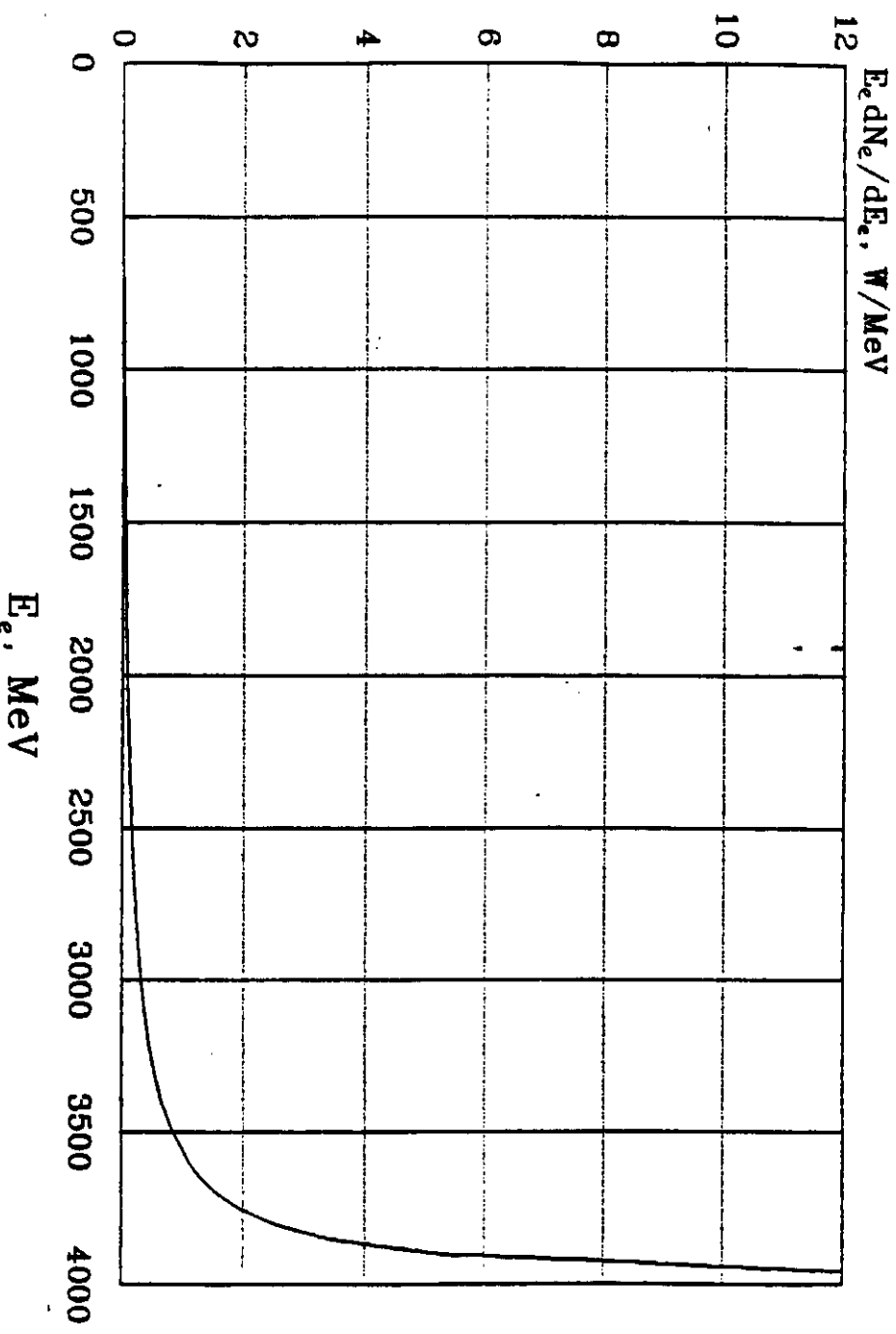


Fig. 8 Spectra of the energy of the beam scattered electrons after passing 0.5 mm thick diamond single crystal.

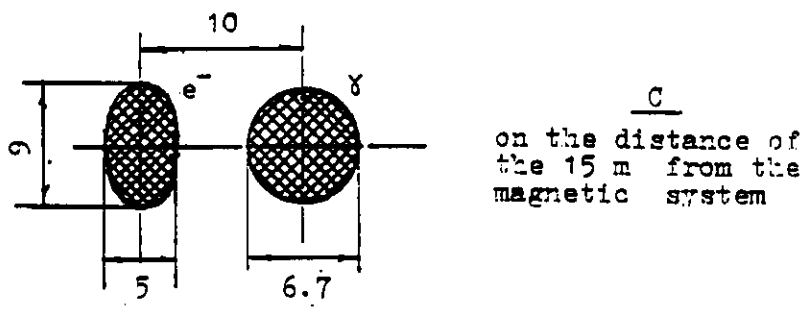
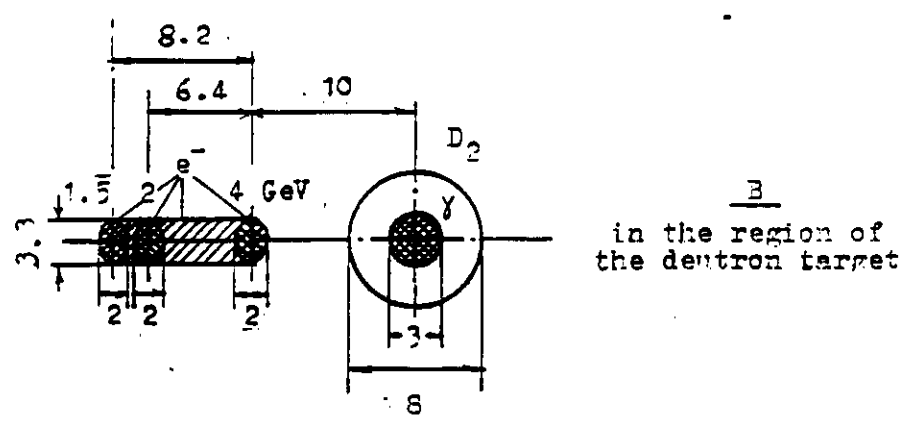
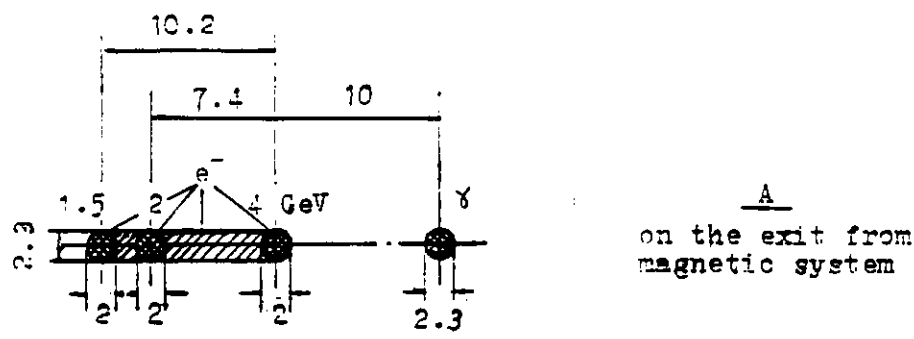


Fig. 9 Arrangement and sizes of the gamma and electron beams on some places of beam line for the diamond crystal 0.5 mm thick. Size of the electron beam before crystal 2 mm, divergence 0.1 mrad.

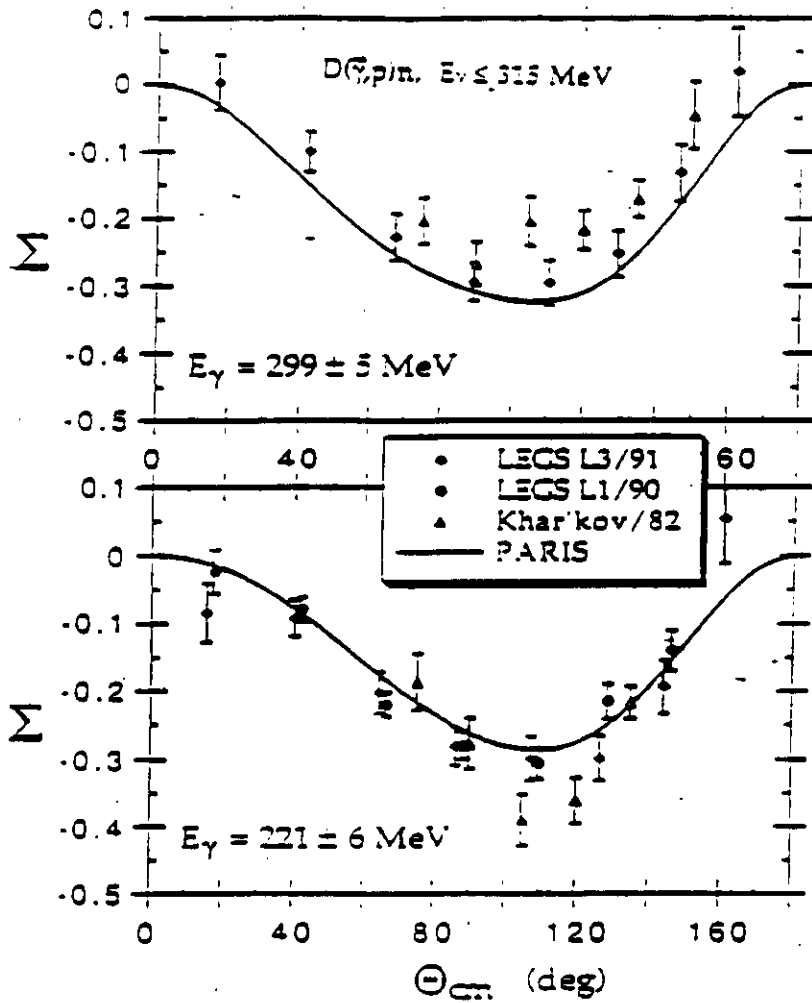


Fig.10 a. The comparison between data from experiments LEGS [19] and Kharkov for the deuteron photoisintegration [15].

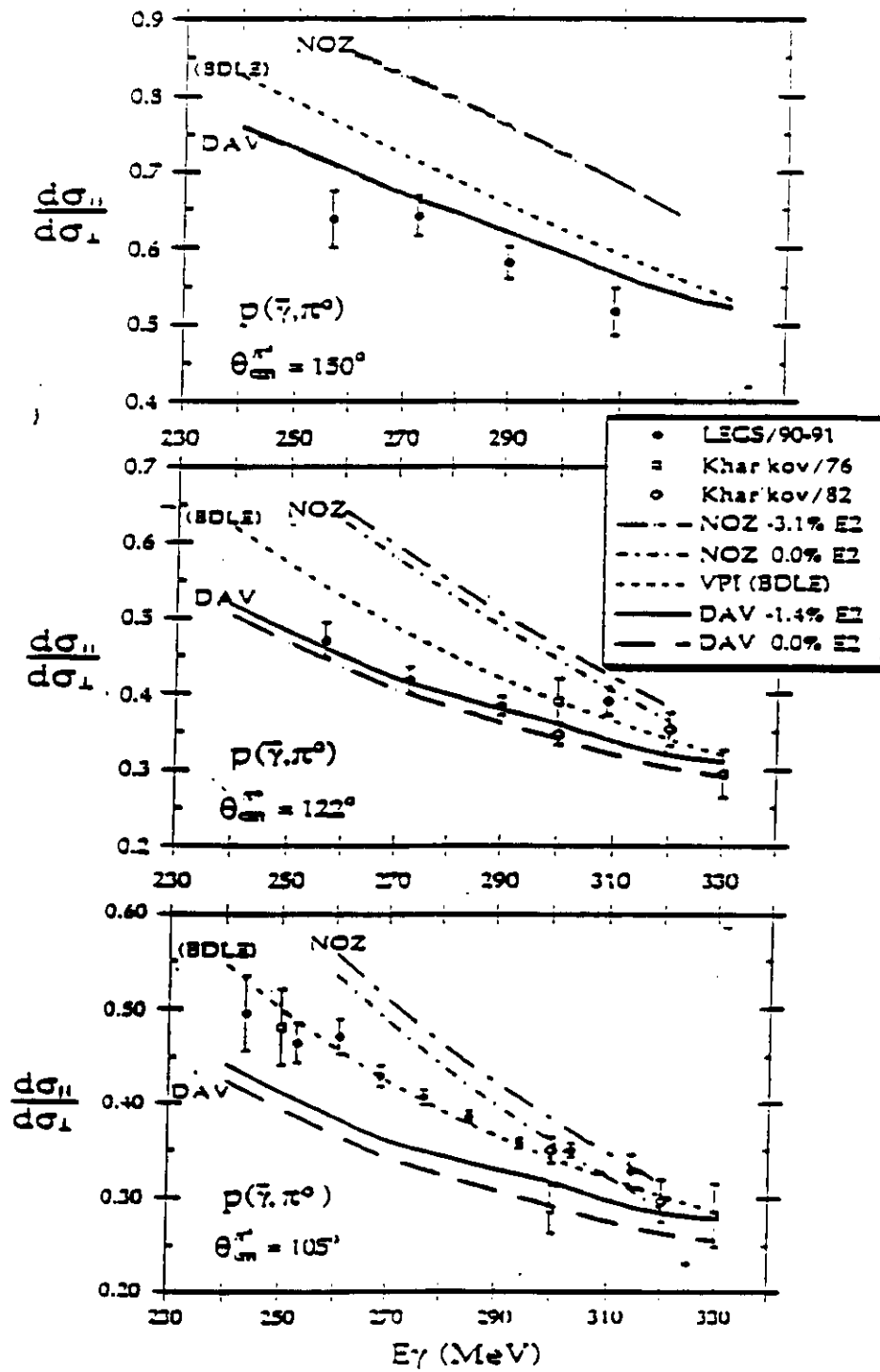


Fig 10 b. The same for π^0 photoproduction [20,21].